

Article

Comparative Study of γ Radiation-Induced Effects on Fiber Bragg Gratings by Femtosecond Laser Point-by-Point Method and Line-by-Line Method

Mingyang Hou ^{1,2,3}, Yumin Zhang ^{1,2,3,*}, Xin Xiong ^{1,2,3} and Lianqing Zhu ^{1,2,3}

¹ Beijing Engineering Research Center of Optoelectronic Information and Instruments, Beijing Information Science and Technology University, Beijing 100192, China

² Beijing Laboratory of Optical Fiber Sensing and System, Beijing Information Science and Technology University, Beijing 100016, China

³ School of Instrument Science and Opto-Electronics Engineering, Beijing Information Science and Technology University, Beijing 100192, China

* Correspondence: yinmin.zhang@gmail.com

Abstract: In the realm of advanced optical fiber sensing (OFS) technologies, Fiber Bragg Grating (FBG) has garnered widespread application in the monitoring of temperature, strain, and external refractive indices, particularly within high-radiation environments such as high-energy physics laboratories, nuclear facilities, and space satellites. Notably, FBGs inscribed using femtosecond lasers are favored for their superior radiation resistance. Among various inscription techniques, the point-by-point (PbP) and line-by-line (LbL) methods are predominant; however, their comparative impacts on radiation durability have not been adequately explored. In this research, FBGs were inscribed on a single-mode fiber using both the PbP and LbL methods, and subsequently subjected to a total irradiation dose of 5.04 kGy (radiation flux of 2 rad/s) over 70 h in a ⁶⁰Co- γ radiation environment. By evaluating the changes in temperature- and strain-sensing performance of the FBG pre-irradiation and post-irradiation, this study identifies a more favorable technique for writing anti-irradiation FBG sensors. Moreover, an analysis into the radiation damage mechanisms in optical fibers, alongside the principles of femtosecond laser inscription, provides insights into the enhanced radiation resistance observed in femtosecond laser-written FBGs. This study thus furnishes significant guidance for the development of highly radiation-resistant FBG sensors, serving as a critical reference in the field of high-performance optical fiber sensing technologies.

Keywords: femtosecond lasers; PbP; LbL; FBG; radiation-resistant



Received: 28 November 2024

Revised: 28 December 2024

Accepted: 31 December 2024

Published: 3 January 2025

Citation: Hou, M.; Zhang, Y.; Xiong, X.; Zhu, L. Comparative Study of γ Radiation-Induced Effects on Fiber Bragg Gratings by Femtosecond Laser Point-by-Point Method and Line-by-Line Method. *Photonics* **2025**, *12*, 32. <https://doi.org/10.3390/photronics12010032>

Copyright: © 2025 by the authors. Licensee MDPI, Basel, Switzerland. This article is an open access article distributed under the terms and conditions of the Creative Commons Attribution (CC BY) license (<https://creativecommons.org/licenses/by/4.0/>).

1. Introduction

Due to its exceptional resistance to electromagnetic interference, miniaturization, high resolution, and accurate measurement of strain and temperature, optical fiber sensing (OFS) technology has been widely utilized in radiation environments such as high-energy physics laboratories, nuclear power plants, and the interior space of artificial satellites. However, the presence of high-energy particles and γ rays in the radiation environment may induce changes in the physical and chemical properties of the fiber material. This includes the generation and proliferation of color centers which can cause radiation damage to the fiber sensor. The cumulative effect of this damage can lead to degradation in the optical performance of the fiber, subsequently impacting the stability of the FBG reflection spectrum and reducing overall performance and reliability of sensing systems. In response

to this challenge, research and development efforts have focused on creating radiation damage-resistant optical fiber sensors. Among these efforts, FBG sensors have garnered significant attention from scientists due to their unique advantages and broad potential for detecting key physical parameters such as temperature, strain, pressure, and displacement.

In order to enhance the radiation resistance of FBG and reduce its radiation effects, researchers are conducting a series of explorations. For example, Shizhe Wen et al. [1] established a model for the generation and elimination of radiation-induced color centers, studying the changes and recovery of the refractive index (RI) of silica FBGs under ^{60}Co - γ radiation. Nirmala Kandadai et al. [2] established a model of FBG sensor based on known experience and demonstrated the RI and spectral changes caused by radiation using numerical methods in the model with different doses of radiation. Jitendra Kumar et al. [3] investigated the radiation effects of I-type, IIa-type, and thermally regenerated FBGs under different-dose radiation from three aspects: center wavelength, reflection intensity, and temperature sensitivity, in Prague. A. Usarov et al. [4] conducted gamma-neutron radiation experiments on single-mode optical fibers coated with copper, aluminum, and polyimide. The results demonstrated that the type of coating can effectively enhance or reduce the radiation sensitivity of FBG. Therefore, it is possible to design radiation-resistant FBGs by adjusting the coating material and thickness. P. F. Kashaykin et al. [5] utilized a femtosecond laser to inscribe FBGs on pure quartz fiber, which was then coated with copper and polyimide coatings before being subjected to a gamma-neutron radiation environment. The findings indicated that in high-dose radiation environments, FBGs written on radiation-resistant fibers with undoped cores and metal protective coatings were the preferred choice. A. Morana et al. [6] utilized an infrared femtosecond laser to inscribe FBGs on germanium-doped, fluorine-doped, and pure quartz fiber core cladding fluorine-doped fibers. These fibers were then subjected to γ radiation with a total dose of 1000 kGy (radiation flux of 50 Gy/s). The experimental findings indicated that the radiation-induced drift in the pure quartz fiber core cladding fluorine-doped fiber was minimal. M. Zaghloul et al. [7] utilized a femtosecond laser to inscribe Type II FBG on pure quartz fiber, which demonstrates resilience in harsh environments characterized by high temperatures of 600 °C and neutron irradiation flux exceeding 1.2×10^{14} n/cm²/s. Baijie Xu et al. [8] utilized the femtosecond laser point-by-point (PbP) technology to fabricate high-temperature-resistant ultra-weak FBG arrays. This array can withstand a high temperature of 1000 °C, and it is expected to be used in harsh environments such as aerospace vehicles and nuclear power plants. Antreas Theodosiou et al. [9] utilized the femtosecond laser PbP and plane-by-plane (PlbPl) methods to engrave the grating, which was then subjected to electron and γ radiation in order to investigate its temperature response. The results indicated that the PlbPl method exhibited superior anti-irradiation performance. Henning Henschel et al. [10] used femtosecond lasers to write I-type FBGs and II-type FBGs on the same optical fiber, and the results proved that the gamma irradiation-induced Bragg wavelength shift (BWS) of II-type FBGs is lower than that of I-type FBGs. Anthony Birri et al. [11] used gamma-neutron radiation to irradiate I-type and II-type Bragg grating arrays in quartz fibers, and the experimental results also showed that the BWS of II-type FBGs is lower than that of I-type FBGs. Therefore, people have reached a consensus that II-type FBGs are generally more resistant to irradiation than I-type FBGs.

In fact, in the application of femtosecond laser direct writing for fabricating FBGs, in addition to the PbP method and the PlbPl method, there is also the line-by-line (LbL) method. In this study, we utilized the infrared femtosecond laser PbP method and LbL method to inscribe FBG on single-mode fiber. The aim of this paper is to investigate the disparity in anti-radiation performance between the two methods in an irradiation environment by testing FBG sensing performance before and after radiation. Furthermore,

we also discuss the advantages of radiation resistance of FBG written by femtosecond laser from a physicochemical properties perspective. The findings of this study not only enhance the potential application of FBG in high-radiation environments but also offer insights for further development of fiber grating technology.

2. Principle

2.1. FBG Sensing Principle

OFS is widely utilized in demanding environments such as aerospace and the nuclear industry due to its resistance to electromagnetic interference, high temperature tolerance, ease of networking, and safety and reliability. FBG stands out as the most common sensor, frequently employed for measuring physical parameters like temperature, pressure, and strain. The sensing principle is illustrated in Figure 1: when broadband light propagates through the fiber, it encounters FBG, where periodic variations in RI within the core cause band-stop filtering. Only light waves satisfying the Bragg condition will undergo reflection; all other waves will continue to transmit as before. Consequently, a distinctive peak will appear on the reflected spectrum. This peak can serve as an observation point for temperature or strain-sensing purposes.

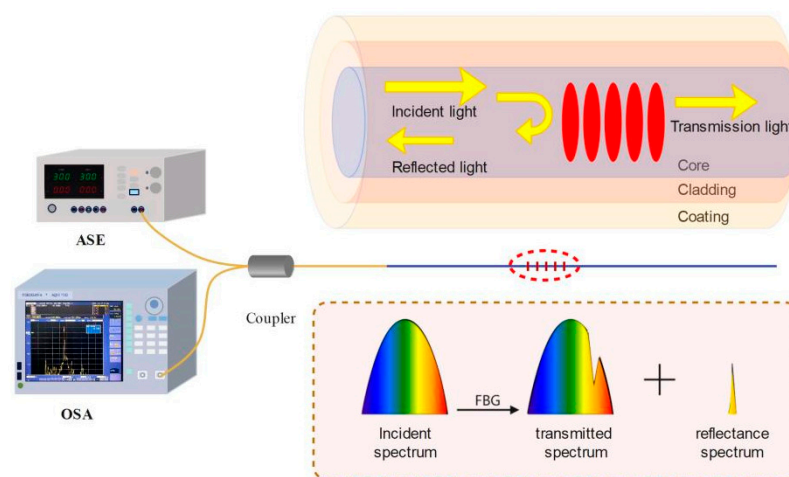


Figure 1. Schematic diagram of FBG sensing principle.

According to the coupled-mode theory, the central wavelength λ_B of the reflection spectrum of FBG mainly depends on the grating period Λ and the effective RI n_{eff} of the reverse coupled mode. Any physical process that changes these two parameters will change the central wavelength λ_B of the reflection spectrum of FBG, that is:

$$m\lambda_B = 2n_{eff}\Lambda \tag{1}$$

In the formula, m is the order of the FBG; λ_B is the central wavelength of the reflection spectrum of FBG; Λ is the grating period of FBG; n_{eff} is the effective RI of the fiber core.

When FBG is affected by external temperature, the effective RI changes due to the thermal expansion effect of the optical fiber, and at the same time, the grating period changes due to the thermal-optic effect. These combined effects result in a drift of the center wavelength of FBG's reflected spectrum. Therefore, by utilizing FBG's response characteristics to temperature, real-time monitoring of the center wavelength of FBG's reflected spectrum can be achieved, and a functional relationship with temperature can be established to obtain the variation in temperature. Similarly, when FBG is subjected to external axial stress, the grating period changes and effective RI changes occur due to the elastic-optic effect. These combined effects also lead to a drift in the center wavelength

of FBG's reflected spectrum. By utilizing FBG's response characteristics to strain, real-time monitoring of FBG's reflected spectrum center wavelength can be achieved, and a functional relationship with strain can be established to obtain variations in strain.

If we do not consider coupling effects between FBG strain and temperature, then the reflection central wavelength of FBG can be expressed as

$$\frac{\Delta\lambda_B}{\lambda_B} = \left\{1 - \frac{n_{eff}^2}{2}[p_{12} - v(p_{11} + p_{12})]\right\}\varepsilon + \left(\alpha + \frac{1}{n_{eff}}\zeta\right)\Delta T \quad (2)$$

In the formula, $\Delta\lambda_B$ is the drift of the center wavelength of the reflection spectrum, p_{11} and p_{12} are the elastic-optic coefficients; v is the Poisson's ratio of optical fiber; ε is the axial strain of the grating, α is the thermal expansion coefficient; ζ is the thermo-optic coefficient; ΔT is the external temperature change. For an FBG of a definite material, its thermo-optic coefficients, coefficient of thermal expansion coefficients, and elasto-optic coefficients are all definite constants.

2.2. FBG Radiation Damage Mechanism and Protection

Optical fibers are frequently exposed to varying levels of radiation in environments such as radiation processing, high-energy physics laboratories, and thermonuclear fusion reactors. The main types of radiation involved include ions, neutrons, and γ rays. Of particular concern are γ rays, which possess strong penetrating power and can still penetrate even after passing through a few-centimeters-thick lead plate. This characteristic has prompted extensive research into the radiation-induced response of optical fibers in such environments over the past few decades.

The radiation effect of optical fiber refers to the changes in sensing performance caused by the alteration of physical and chemical properties when the fiber interacts with radiation. Therefore, in order to investigate the mechanism of fiber radiation-induced damage, it is essential to begin with an understanding of the basic physical and chemical properties of the fiber. The fiber is primarily composed of amorphous SiO_2 , which exists in a disordered network of $\text{Si}(\text{O}_{1/2})_4$ tetrahedrons. In a radiation environment, the fiber undergoes discoloration, hardening, and increased brittleness due to structural defects introduced during production such as intermediates, suspension bonds, and peroxide connections. These defects lead to ionization and generation of numerous free electron-hole pairs. These electron-hole pairs are captured by pre-existing intrinsic defects (such as oxygen vacancy centers, peroxy junctions, and peroxy radicals), doping, and impurity defects (such as SiOH) within the fiber. This results in the formation of new charged defect structures that can trap electrons and holes. Consequently, this triggers excitation of electrons and holes within the fiber, leading to increased radiative loss.

In addition, during the production process of the fiber, various ions may be intentionally or unintentionally doped, leading to the presence of impurity ions such as Cl ions, OH ions, and colored ions of Fe, Cr, Mn, Cu, Co, Ni, Pb. Under the influence of γ radiation, these impurity ions will generate a P1 defect structure and associated holes in the fiber and form a new wavelength-absorption center known as a color center [12,13]. As a result of this phenomenon, conventional germanium-doped single-mode fiber is susceptible to RIA in high-radiation environments. This susceptibility is mainly attributed to the fact that rare earth element co-admixture added during production can disrupt the basic network structure of SiO_2 and lead to relatively unstable chemical bonds. In a radiation environment, this unstable structure tends to produce more defects and color centers. Consequently, pure quartz core fiber exhibits better resistance against radiation in such environments due to its lack of added impurities. The formation of color centers is typically associated with

changes in internal density within the fiber and FBG, as well as changes in RI, which results in increased absorption at specific wavelengths, causing RIA.

Therefore, it is crucial to investigate the formation mechanism of color centers. Among these, the E' color center is the most commonly detected point defect structure and has been extensively studied over a long period of time. Oxygen vacancy defects are generally considered to be the primary cause of E' color center formation [14,15]. Some of these defects originate from the manufacturing process of optical fibers, while others are generated during irradiation. Low-energy radiation particles mainly induce the generation of E' color centers through ionization effects on intrinsic defects, whereas high-energy radiation particles primarily cause lattice structure defects through fatigue fracture of silicon dioxide lattice or displacement of oxygen atoms, leading to the formation of E' color centers [16].

In consideration of the generation of E' color centers, researchers have proposed pre-radiating the optical fiber. Pre-radiation of the optical fiber allows for the formation of a more stable SiO_2 lattice structure, significantly reducing its sensitivity to subsequent radiation, a phenomenon known as radiation hardening [17,18]. Additionally, pre-high temperature treatment can enhance the radiation resistance of the fiber by eliminating easily activated free radicals, atomic defects, or relaxation bonds and converting them into stable bonds at high temperatures [19]. Subsequent cold annealing treatment serves to reduce the activation energy of the material and promote a more orderly molecular arrangement while decreasing internal defect structures, ultimately reducing the radiation sensitivity of quartz fiber [20,21].

Therefore, it is evident that the anti-irradiation ability of optical fibers primarily depends on both their material composition and pretreatment methods prior to irradiation.

2.3. The Principle of Femtosecond Writing FBG

The anti-irradiation performance of FBG is not only influenced by the radiation effect of the fiber itself, but also depends on the characteristics of the FBG. Among these factors, the writing technology of FBG is a core determinant of its radiation resistance. Utilizing a femtosecond laser to write FBG can effectively enhance the radiation resistance and stability of FBG in harsh environments. The femtosecond laser pulse is characterized by an ultra-short pulse width and ultra-high power peak. When it is focused on the optical fiber core, the laser energy can be concentrated into a very small area within a time scale shorter than the lattice thermal diffusion time. This instantaneous deposition of high-density energy will fundamentally alter the absorption and movement of electrons in the material, leading to a strong nonlinear effect. Two important nonlinear excitation mechanisms are involved: "photoionization" and "avalanche ionization". Photoionization includes multi-photon ionization and tunnel ionization [20]. Taking standard single-mode germanium-doped silicon dioxide fiber as an example, the band gap E_g reaches 7.1 eV. The central wavelength of the infrared femtosecond laser is 800 nm, and the energy of the associated photon is 1.55 eV. Sufficient energy is required to cross the band gap in order to achieve the transition from valence to conduction band. This necessitates a five-photon absorption process during nonlinear absorption, which results in multi-photon ionization. Tunnel ionization occurs when the intensity of the incident femtosecond laser is increased to 10^{13} W/cm^2 [22], causing the alternating electric field generated by the femtosecond laser energy field and the Coulomb field between the molecule and valence electron to superimpose on each other. As a result, this distortion greatly reduces the Coulomb barrier of electrons between molecules and valence electrons. Due to the tunneling effect, valence electrons within this severely distorted Coulomb barrier can completely break away from atoms and become free electrons through a process known as tunneling ionization. Subsequently, the conduction band electron increases its energy by continuously absorbing the photon energy of the

incident femtosecond laser. When its energy reaches a certain threshold, it can excite the valence electron from the valence band to the conduction band through collision, resulting in two conduction band electrons. This process, known as avalanche ionization, leads to a rapid increase in the number of conduction band electrons. Under this series of absorption and ionization processes, local defects and damage occur in the optical fiber material [23], leading to changes in its RI.

The interaction between femtosecond lasers and fiber materials involves not only nonlinear effects such as two-photon absorption and multi-photon absorption, but also includes threshold effects [24]. This effect indicates that defects can occur in the fiber only when the laser energy reaches or exceeds a certain value. Once the laser energy reaches or exceeds this threshold, irradiating the core of an ordinary single-mode fiber triggers avalanche ionization, resulting in a free electron plasma that leads to highly localized deposition of energy in the nearby region. Within a few picoseconds, the electron energy excited by the femtosecond laser will be transferred to the lattice of the region of action. After a few picoseconds, the material on one side of the laser core will melt, rapidly solidify, and contract, resulting in a local density change on one side of the core. This forms a structure related to the laser polarization and results in material damage or lattice distortion [25]. This process induces permanent RI modulation in and around the unilateral region of optical fiber core. The modulation causes a RI change of more than 10^{-2} and is also referred to as core modification.

Therefore, the periodic use of a femtosecond laser at the position of the fiber core can induce modifications to the fiber core material. This results in the occurrence of two-photon absorption, multi-photon absorption, and nonlinear effects, leading to periodic changes in the RI at the fiber core. The resulting permanent damage manifests as stable FBG formations.

3. Experimental Results and Discussion

3.1. Femtosecond Writing FBG Device

The schematic diagram of the FBG system for femtosecond laser writing is depicted in Figure 2 below. The system comprises a femtosecond laser, half-wave plate, Gran prism, pinhole diaphragm, shutter, mirror, oil mirror, camera, 3D displacement platform, ASE light source, and OSA. The central wavelength of the femtosecond laser is 800 nm, with a repetition rate of 1 kHz and a pulse width of 35 fs. The laser passes through a combination of a half-wave plate and a Gran prism before entering the aperture. It then goes through the shutter and mirror reflection into the $63\times$ oil lens. By utilizing matching fluid between the oil lens and oil mirror, the laser is focused on the optical fiber core position through the cladding. Subsequently, using a charge-coupled device (CCD), the position for laser writing is determined while monitoring real-time processing status of the FBG. The period of the FBG can be changed by changing the moving speed of the 3D displacement table, and the central wavelength of the FBG can be affected. In this experiment, femtosecond laser was used to write FBG on Corning's SMF-28 fiber by the PbP method and LbL method for comparison experiment.

The setting parameters are as follows: the period of writing grating by the PbP method is 548 nm, which belongs to the I-type FBG, and the length of writing interval is 3 mm; the LbL writing cycle is $1.071\ \mu\text{m}$, which belongs to the II-type FBG; each line length is $6\ \mu\text{m}$, the same as the optical fiber core diameter; the number of lines is 3000; the length of the grid area is approximately 3 mm. As shown in Figure 3, the PbP method of FBG writing is to place the fiber to be written on the displacement platform, and the femtosecond laser passes through the fiber cladding and coating layer, focusing on the position of the optical fiber core. The fiber moves 3 mm along the X-axis with the shutter quickly opening and

closing, and FBG writing can be completed by the PbP method. The fiber to be written by the LbL method is also placed on a displacement platform, and then the position is adjusted so that the femtosecond laser passes through the fiber cladding and coating layer to focus on the optical fiber core position. When the shutter is open, the fiber is moved down the Y-axis by 6 μm , and line 1 is carved in the optical fiber core. Then the shutter is closed and the fiber moves 1.075 μm along the X-axis. Then the fiber is moved 6 μm up the Y-axis and line 2 is written in the optical fiber core. Then the shutter is closed and the fiber moves 1.075 μm along the X-axis. After that, by repeating the above steps 1500 times, FBG can be written by the LbL method, and the length of the grid area is also approximately 3 mm.

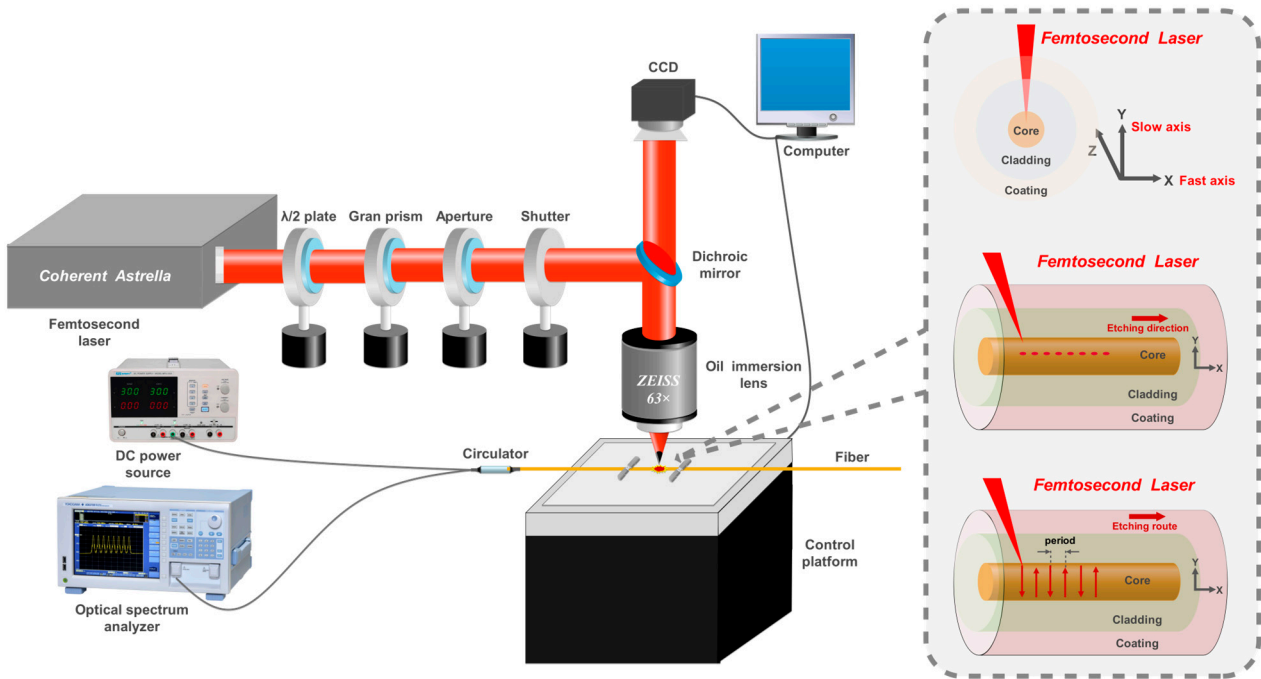


Figure 2. Schematic of femtosecond inscription FBG.

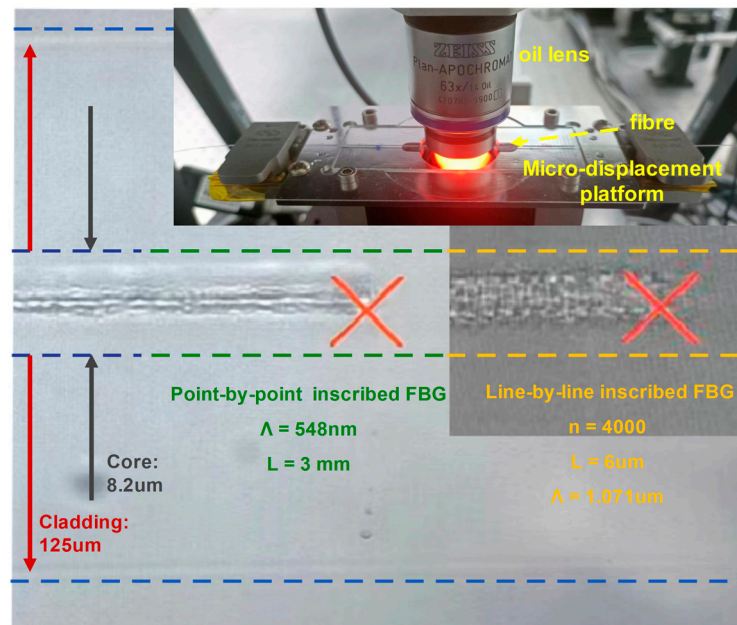


Figure 3. Micrograph of writing FBG by femtosecond laser.

3.2. Sensing Experimental System

In the temperature–strain two-parameter sensing experiment, a system is used that consists of a broadband light source (BBS) spanning from 1525 nm to 1625 nm, an OSA with a wavelength resolution of 0.02 nm (Yokogawa, Tokyo, Japan), a strain platform, and a heating platform. The OSA records the reflection spectrum. The schematic diagram of the sensing experimental system is shown in Figure 4, and the sensing experiment diagram is shown in Figure 5.

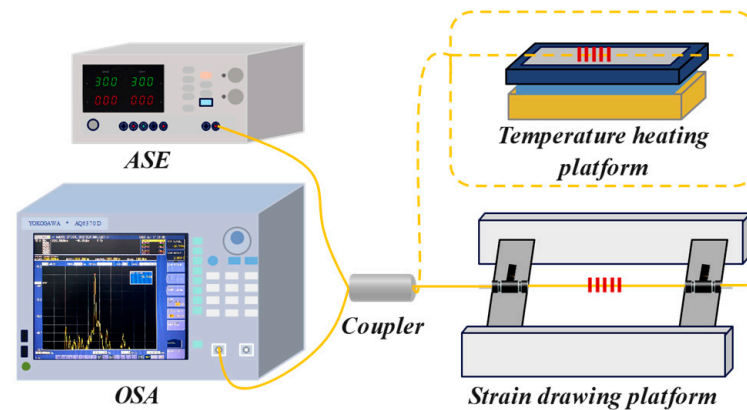


Figure 4. Schematic of sensing experiment.



Figure 5. Sensing experiment setup.

Firstly, the sensor is placed on the heating platform and fixed. The center wavelength of FBG is measured at room temperature of 20 °C, and then the temperature is raised to 50 °C. After the temperature is stabilized for 10 min, the center wavelength is measured again, and the spectrum is recorded. Then, the above operation is repeated every 50 °C until the heating temperature reaches 450 °C. Finally, the center wavelength of FBG in the stable state during the heating process is measured. After that, the central wavelength of the FBG at 450 °C is measured again as the starting point of the cooling process. Measurements are then taken every 50 °C until the temperature of the heated platform reaches 20 °C. At this point, a complete temperature-sensing experiment is completed.

After that, the sensor is placed at the center of the strain platform, and prestress is applied to ensure that the fiber is stretched straight and can be directly applied to the fiber when axial stress is applied later, and then it is fixed on the strain platform. The original length L of the strain platform is 40 cm. After rotating the knob at the right end of the strain platform by 10 μm , the strain platform will move 0.1 mm to the right, denoted as

ΔL . The axial stress calculation formula shows that $250 \mu\epsilon$ is generated. The starting point is that the sensor is just fixed on the strain platform, and the spectrum is recorded every $250 \mu\epsilon$ until the axial strain applied by the strain platform reaches $2000 \mu\epsilon$, the spectrum is recorded for the last time, and the stress application process is completed. After that, the spectrum of the sensor applied with $2000 \mu\epsilon$ axial strain is recorded again, and the spectrum is recorded once for every $250 \mu\epsilon$ reduction until the axial strain on the strain platform is $0 \mu\epsilon$. During the whole process, the temperature of the sensing area remains unchanged when the loading strain and unloading strain are guaranteed. It must be ensured that the strain of the sensing area remains unchanged when heating and cooling.

After the FBG sensor is radiated, the sensing experiment is carried out again in the same way, and the data is recorded. During the experiment, ^{60}Co - γ radiation will ionize or excite biological macromolecules in the human body, so that they can be modified, which will cause irreversible damage to the human body. Therefore, for the current experimental conditions, it is not possible to perform temperature- and strain-sensing experiments on FBGs in a real radiation environment. Waiting for the radiation to end, the complete fiber optic sensing experiment was immediately taken out to ensure the validity of the radiation resistance comparison experiment. Due to the lag analysis of the experiment, it is impossible to repeat the sensing experiment before and after radiation.

3.3. Radiation Experiment

Due to the complexity of the radiation environment, there are numerous factors that influence the radiation resistance of FBG. These factors include the material of the fiber, the working wavelength, and the method used to create the FBG. The FBG was placed in a γ ray environment generated by ^{60}Co to assess its radiation resistance. This is because ^{60}Co - γ rays exhibit superior performance compared to other radiation sources and are widely utilized in testing radiation environments due to their iconic applicability. Our target environments for this study include high-energy physics laboratories, nuclear power plants, and high-radiation areas such as inside satellites. The experimental protocol was designed to evaluate the performance of FBG in a medium-to-high-dose radiation environment. In this experiment, it was placed in a radiation environment with a radiation dose of 5.04 kGy (radiation flux of 2 rad/s) for 70 h . This approach allows us to effectively assess the radiation resistance of the FBG sensor under extreme conditions.

This experiment was supported by the facilities provided by the Key Laboratory of Radiopharmaceuticals at Beijing Normal University. These facilities include a continuously operating ^{60}Co - γ radiation source system, shielding screens to prevent radiation leakage, and an independent and enclosed laboratory environment. As shown in Figure 6, during the experiment, the bare fiber to be tested is bound side-by-side on the titanium plate, facing the ^{60}Co - γ radiation source. The optical fiber is not pre-treated for radiation protection, in order to ensure that all FBG sensors receive a uniform intensity of radiation. Immediately after completing the radiation exposure, sensing performance tests are performed on the fiber to evaluate the radiation resistance of FBG made by different inscription technologies in high-radiation environments. This method ensures accuracy and reliability of experimental results.

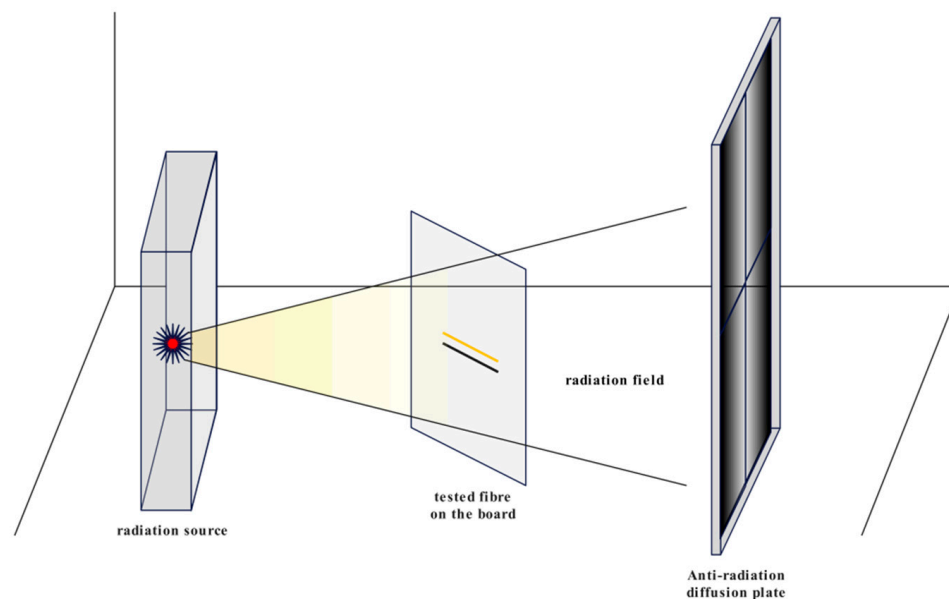


Figure 6. Schematic of radiation experiment.

3.4. Experimental Analysis

The temperature- and strain-sensing experiments of FBG were conducted using the PbP method and LbL method before and after radiation exposure. The reflectivity spectra of FBG were recorded and analyzed to create a 3D waterfall diagram illustrating the temperature- and strain-sensing performance of FBG written by the PbP method. Additionally, a central wavelength drift diagram was generated through peak analysis to visually demonstrate the performance change of FBG before and after radiation. This paper presents temperature-sensing spectrograms and central wavelength drift diagrams (Figures 7 and 8), as well as strain-sensing spectrograms and central wavelength drift diagrams (Figures 9 and 10) of FBG written by the PbP method before and after radiation exposure, respectively. As the spectral characteristics of FBG written by the LbL method are similar to those produced by the PbP method, a large number of diagrams are not repeated in this study.

In order to facilitate comparison and observation of the changes in sensor performance before and after radiation using the two FBG writing methods, we have organized the data of key performance indicators, such as linearity, maximum error, and sensor sensitivity, and summarized these data in Table 1. Furthermore, to visually demonstrate the decrease in sensing performance due to radiation, we created Table 2 to clearly illustrate the specific impact of radiation on FBG sensing performance.

Table 1. Comparison of sensing performance parameters in FBGs written by the PbP and LbL method before and after radiation.

Type	Status	R ² of Heating	Maximal Error of Heating	R ² of Cooling	Maximal Error of Cooling	R ² of Applied Strain	Maximal Error of Applied Strain	R ² of Unloading Strain	Maximal Error of Unloading Strain	Temperature Measurement Resolution (pm/°C)	Strain Measurement Resolution (pm/με)
PbP	before radiation	0.99533	0.27052	0.99304	0.24199	0.99936	0.03483	0.99906	0.03044	11.62	1.15
	after radiation	0.99152	0.31484	0.98952	0.3388	0.99593	0.08511	0.99617	0.11178	11.73	1.15
LbL	before radiation	0.99436	0.26805	0.99427	0.40633	0.99979	0.02489	0.99933	0.03689	12.31	1.13
	after radiation	0.98516	0.3253	0.92358	0.6645	0.99568	0.07867	0.99561	0.08289	11.95	1.15

Table 2. Comparison of sensing performance attenuation parameters in FBGs inscribed by the PbP and LbL method before and after radiation.

Type	ΔR ² of Temperature	ΔMaximal Error of Temperature	ΔR ² of Strain	ΔMaximal Error of Strain	Temperature Measurement Resolution After Radiation (pm/°C)	ΔTemperature Measurement Resolution Ratio	Strain Measurement Resolution After Radiation (pm/με)	ΔStrain Measurement Resolution Ratio
PbP	−0.00381	+0.04432	−0.00343	+0.05028	11.73	0.9%	1.15	0
LbL	−0.0092	+0.05725	−0.00411	+0.05378	11.95	2.92%	1.15	1.8%

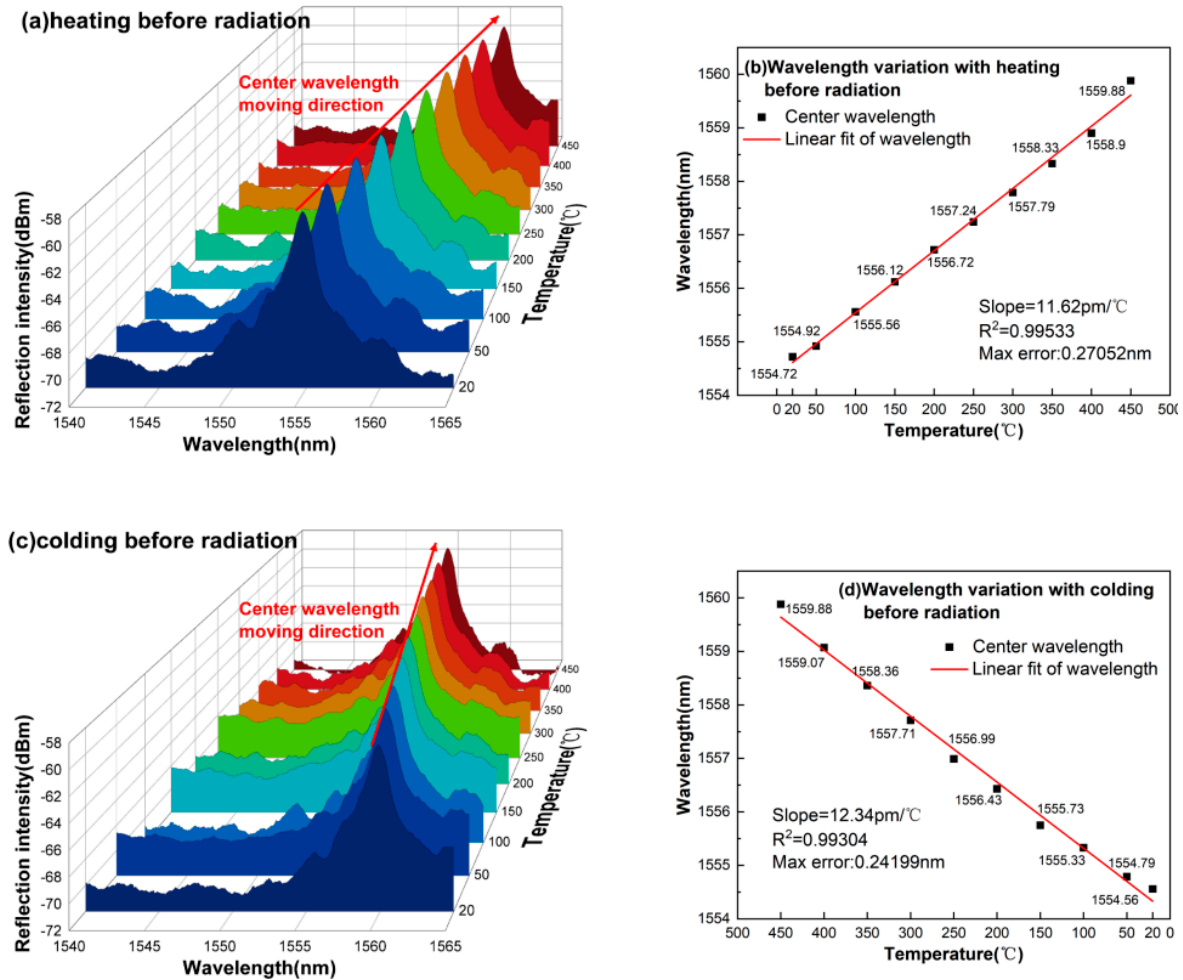


Figure 7. Temperature-sensing spectral diagram and central wavelength drift diagram written by the PbP method before irradiation: (a) 3d spectrum of heating; (b) center wavelength drift diagram of heating; (c) 3d spectrum of cooling; (d) center wavelength drift diagram of cooling.

Upon observing Tables 1 and 2, it is evident that the temperature sensitivity of FBG is significantly higher than its strain sensitivity regardless of the writing method used. This highlights the considerable advantage of FBG in temperature monitoring. Consequently, this feature provides a clear direction for designing temperature–strain two-parameter sensors that can be optimized for temperature-sensing applications by effectively encapsulating FBG to minimize the impact of radiation on its performance. Furthermore, under the same radiation conditions, the BWS inscribed by the PbP method is 0.16 nm, which is smaller than that of the LbL method, which is 0.44 nm, even when the FBG written by the PbP method belongs to the I-type FBG, and the FBG written by the LbL method belongs to the II-type FBG. Upon examining the data in Tables 1 and 2 under identical radiation conditions, it is found that the FBGs written using the PbP method not only have smaller BWS, but also exhibit less performance degradation in terms of resolution changes in temperature and strain, as well as demonstrating better linearity and maximum error compared to those written using the LbL method. This suggests that the PbP method offers superior resistance to radiation effects. We speculate that the physical mechanism behind the better radiation resistance of the PbP method may be due to the combined effects of the following two reasons: (1) Due to the relatively small etching area of the PbP method, its cumulative effect when exposed to the irradiation environment is also smaller. This leads to a reduction in the heterogeneity at the microstructure level of the FBG after

inscription, that is, it alleviates the microstructure perturbations induced by irradiation. Such independent exposure at single points reduces the overall cumulative effect of the refractive index distribution caused by radiation, which is conducive to maintaining the stable performance of the FBG. (2) The process of inscribing an FBG with the femtosecond laser PbP technique involves altering the refractive index of the fiber core at individual points, resulting in a more uniform and orderly internal structure of the FBG. Each point of laser interaction operates independently and precisely, facilitating the formation of a more regular region of refractive index modulation within the fiber core. Conversely, the LbL method creates the grating through a continuous axial scan along the fiber, which, due to the continuity of the laser scanning path, may lead to concentration of defects, stress, and non-uniform distribution of localized heat accumulation. When exposed to radiation, the thermal effects generated by irradiation can intensify structural changes in regions of energy non-uniformity present within gratings produced by LbL methods. Furthermore, particles generated by radiation, such as ions in high-energy beams, may interact with these defects, causing additional material damage, such as localized chemical bond breakage or color center formation. In comparison, the PbP method, with its relatively regular structure and more dispersed distribution of induced defects, stress, and heat, is better able to withstand the adverse effects of radiation, thus exhibiting superior radiation-resistant performance.

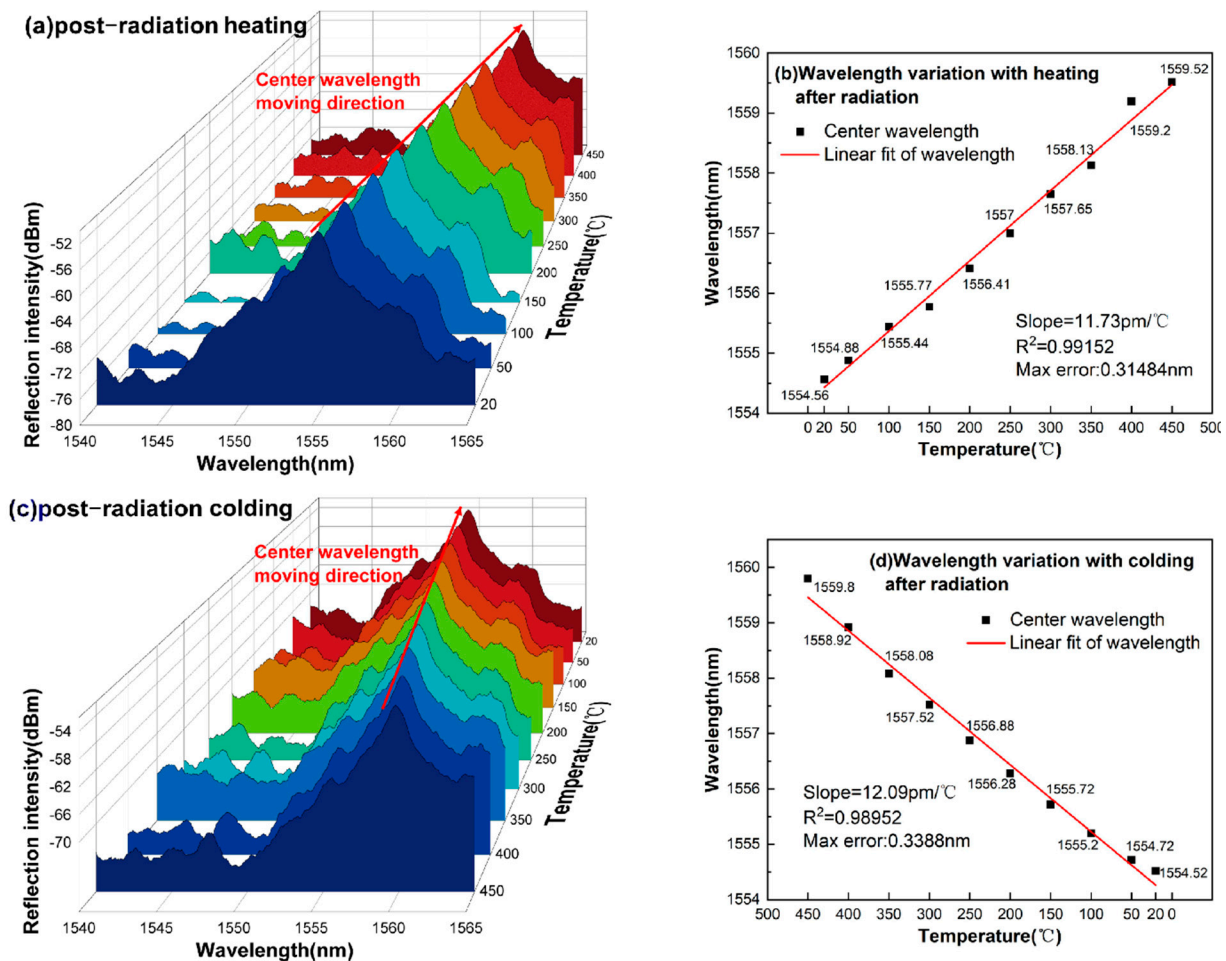


Figure 8. Temperature-sensing spectral diagram and central wavelength drift diagram written by the PbP method after irradiation: (a) 3d spectrum of heating; (b) center wavelength drift diagram of heating; (c) 3d spectrum of cooling; (d) center wavelength drift diagram of cooling.

In addition, by summarizing the radiation effect of optical fiber and the related research on the principle of femtosecond laser-written FBG, the reasons for the strong anti-

irradiation performance of femtosecond laser-writing technology compared with other writing methods mainly include the following reasons: (1) The extremely short pulse width of a femtosecond laser enables high energy to be focused in a very short time in a tiny area of the fiber, accurately modifying the material structure inside the fiber without affecting the surrounding area. This results in high-quality, high-stability grating when combined with femtosecond laser-written FBG. The peak power of the femtosecond laser can produce strong nonlinear effects, which can create stable modified structures near the fiber core and have high disturbance resistance to external environmental changes. (2) Femtosecond lasers can be directly written on non-photosensitive fibers, such as pure quartz fibers. The fiber material itself is difficult to produce color centers in, compared to other doped fibers, thus reducing the radiation effect caused by color center proliferation. (3) When a femtosecond laser writes an FBG at its core, it will be accompanied by changes in physical and chemical properties, such as changes in RI and radiation densification. In a sense, this is also a pre-radiation process. The radiation effect caused by $^{60}\text{Co}-\gamma$ radiation can be effectively weakened through radiation hardening to inhibit defect formation. Therefore, femtosecond laser-written FBGs exhibit excellent anti-irradiation performance.

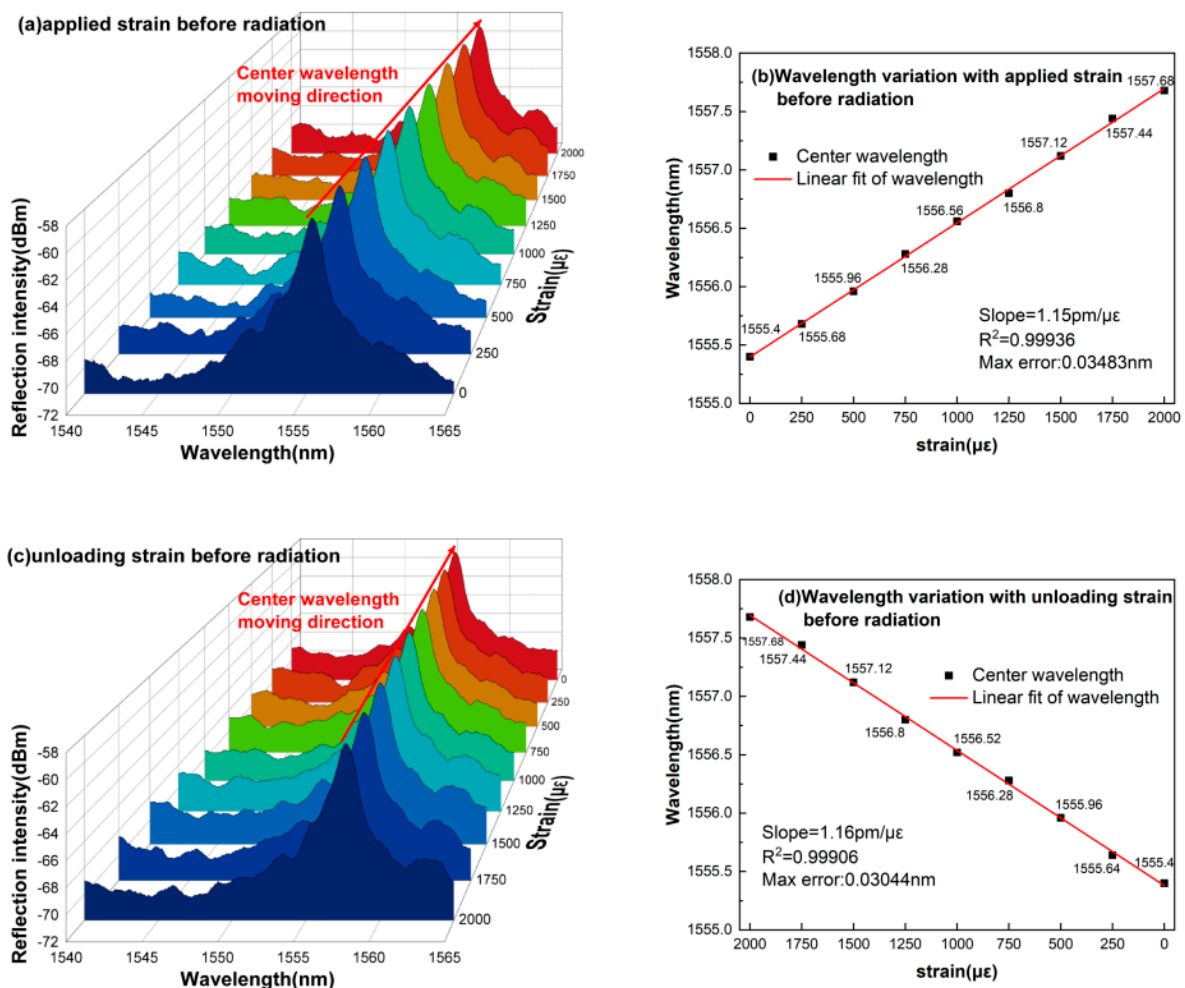


Figure 9. The strain-sensing spectrum and the central wavelength drift diagram written by the PbP method before irradiation: (a) 3d spectrum of applying strain; (b) center wavelength drift diagram of applying strain; (c) 3d spectrum of unloading strain; (d) center wavelength drift diagram of unloading strain.

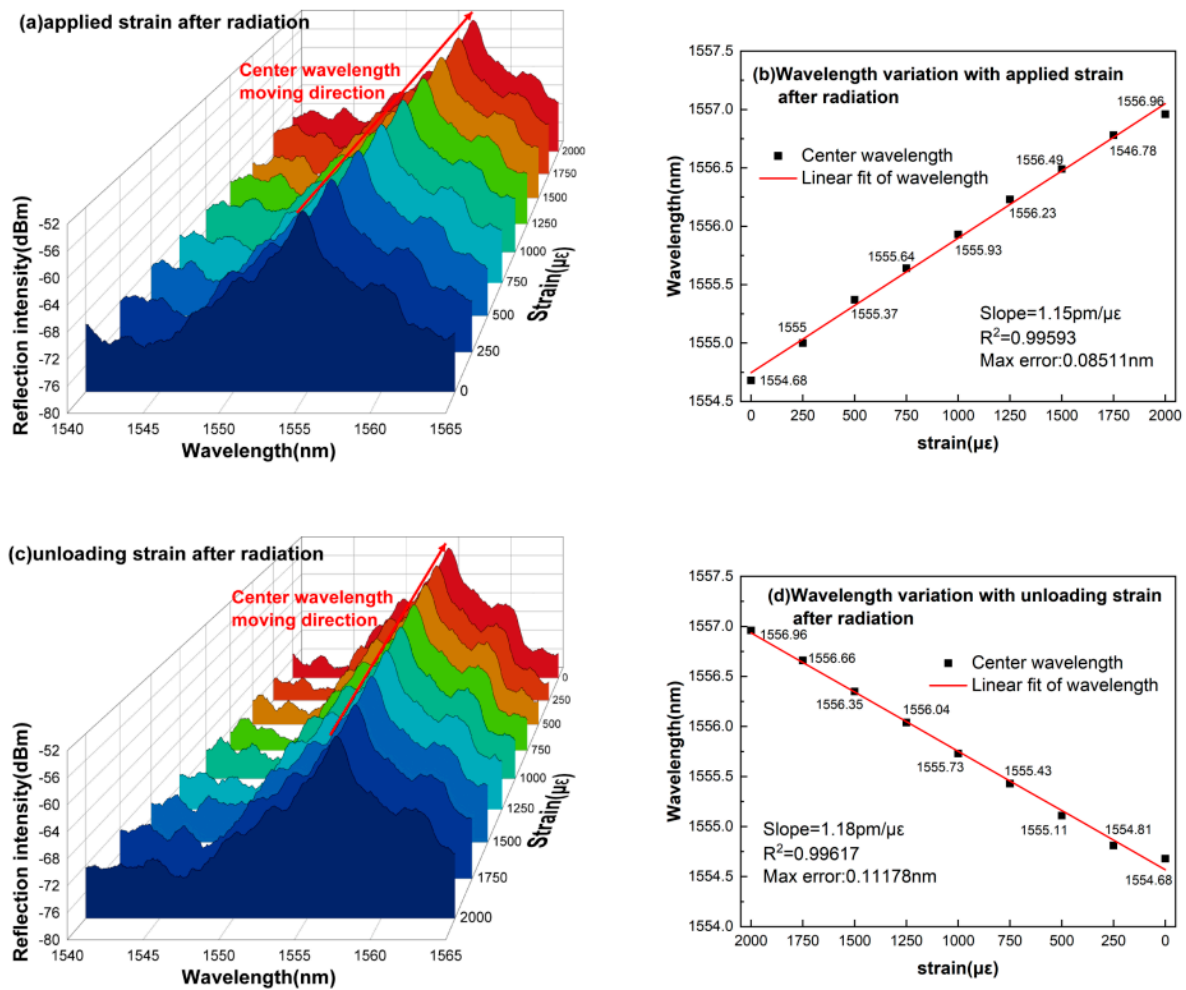


Figure 10. The strain-sensing spectrum and the central wavelength drift diagram written by the PbP method after irradiation: (a) 3d spectrum of applying strain; (b) center wavelength drift diagram of applying strain; (c) 3d spectrum of unloading strain; (d) center wavelength drift diagram of unloading strain.

4. Conclusions

In this study, we investigate the impact of different femtosecond laser-writing techniques on the radiation resistance of FBG sensors. Our goal is to identify the most suitable fabrication method for enhancing the stability of FBG sensors in high-radiation environments. In our experiment, FBGs were inscribed on single-mode fiber using femtosecond laser PbP and LbL methods. Subsequently, the FBG sensors were exposed to ^{60}Co - γ radiation at a total dose of 5.04 kGy in their bare fiber state. The sensing performance of the FBG sensors was thoroughly evaluated before and after irradiation. The experimental findings reveal that (1) FBGs written using the PbP method exhibit significantly better radiation resistance compared to those written using the LbL method; (2) FBGs inscribed with a femtosecond laser demonstrate greater sensitivity to temperature changes. Furthermore, we provide an explanation for the robust anti-irradiation performance observed in FBGs written with a femtosecond laser technique.

This study not only validates the efficacy of femtosecond laser PbP writing technology in enhancing the anti-radiation performance of FBG sensors, but also serves as a crucial reference for technology selection and improvement of the anti-radiation performance of temperature and strain dual-parameter sensors. This will significantly advance the application of FBG sensors in high-radiation fields such as the nuclear industry and aerospace.

Author Contributions: Conceptualization, M.H. and Y.Z.; methodology, M.H.; data curation, X.X.; writing—original draft preparation, M.H.; writing—review and editing, M.H.; supervision, Y.Z.; project administration, Y.Z.; funding acquisition, L.Z. All authors have read and agreed to the published version of the manuscript.

Funding: This work was supported by the Research Project of Beijing Municipal Natural Science Foundation (No. BJXZ2021-012-00046).

Institutional Review Board Statement: Not applicable.

Informed Consent Statement: Not applicable.

Data Availability Statement: All data that support the findings of this study are included within the article.

Conflicts of Interest: All authors do not have any potential conflicts of interest.

References

1. Wen, S.-Z.; Xiong, W.-C.; Huang, L.-P.; Wang, Z.-R.; Zhang, X.-B.; He, Z.-H. Damage and recovery of fiber Bragg grating under radiation environment. *Chin. Phys. B* **2018**, *27*, 090701. [\[CrossRef\]](#)
2. Rana, S.; Subbaraman, H.; Fleming, A.; Kandadai, N. Numerical Analysis of Radiation Effects on Fiber Optic Sensors. *Sensors* **2021**, *21*, 4111. [\[CrossRef\]](#) [\[PubMed\]](#)
3. Kumar, J.; Prakash, O.; Kumar, S.; Dixit, S.K.; Bhardwaj, Y.K.; Nakhe, S.V. Effect of gamma radiation dose on the performance of negative-index fiber Bragg gratings. *Opt. Eng.* **2019**, *58*, 057108. [\[CrossRef\]](#)
4. Gussarov, A.; Chojetzki, C.; Mckenzie, I.; Berghmans, F. Influence of the coating type on the radiation sensitivity of FBGs. In *Optical Sensors 2008*; Bergmans, F., Mignani, A.G., Cutolo, A., Meyrueis, P.P., Pearsall, T.P., Eds.; SPIE: Bellingham, WA, USA, 2008; Volume 7003, p. 700309. [\[CrossRef\]](#)
5. Kashaykin, P.F.; Vasiliev, S.A.; Tomashuk, A.L.; Ignatyev, A.D.; Britskii, V.A.; Shaimerdenov, A.A.; Akhanov, A.M.; Silnyagin, P.P.; Kulsartov, T.V. Radiation Resistance of Fiber Bragg Gratings under Intense Reactor Irradiation. *Bull. Lebedev Phys. Inst.* **2023**, *50* (Suppl. S3), S322–S328. [\[CrossRef\]](#)
6. Morana, A.; Girard, S.; Marin, E.; Marcandella, C.; Périsset, J.; Macé, J.R.; Boukenter, A.; Cannas, M.; Ouerdane, Y. Radiation hardening of FBG in harsh environments. In Proceedings of the SPIE 9157, 23rd International Conference on Optical Fibre Sensors 9157, Santander, Spain, 2–6 June 2024; Mirapeix, S., Jesus, M., Eds.; SPIE-International Society of Optical Engineering: Bellingham, WA, USA, 2014; p. 91578. [\[CrossRef\]](#)
7. Zaghoul, M.A.; Wang, M.; Huang, S.; Hnatovsky, C.; Grobncic, D.; Mihailov, S.; Li, M.-J.; Carpenter, D.; Hu, L.-W.; Daw, J.; et al. Radiation resistant fiber Bragg grating in random air-line fibers for sensing applications in nuclear reactor cores. *Opt. Express* **2018**, *26*, 11775. [\[CrossRef\]](#)
8. Xu, B.; He, J.; Du, B.; Xiao, X.; Xu, X.; Fu, C.; He, J.; Liao, C.; Wang, Y. Femtosecond laser point-by-point inscription of an ultra-weak fiber Bragg grating array for distributed high-temperature sensing. *Opt. Express* **2021**, *29*, 32615. [\[CrossRef\]](#) [\[PubMed\]](#)
9. Theodosiou, A.; Leal-Junior, A.; Marques, C.; Frizzera, A.; Fernandes, A.J.S.; Stancalie, A.; Ioannou, A.; Ighigeanu, D.; Mihalcea, R.; Negut, C.D.; et al. Comparative Study of γ - and e-Radiation-Induced Effects on FBGs Using Different Femtosecond Laser Inscription Methods. *Sensors* **2021**, *21*, 8379. [\[CrossRef\]](#)
10. Henschel, H.; Hoeffgen, S.K.; Krebber, K.; Kuhnhen, J.; Weinand, U. Influence of fiber composition and grating fabrication on the radiation sensitivity of fiber Bragg gratings. In Proceedings of the 2007 9th European Conference on Radiation and Its Effects on Components and Systems, Deauville, France, 10–14 September 2007; pp. 1–8. [\[CrossRef\]](#)
11. Birri, A.; Wilson, B.A.; Blue, T.E. Deduced Refractive Index Profile Changes of Type I and Type II Gratings When Subjected to Ionizing Radiation. *IEEE Sens. J.* **2019**, *19*, 5000–5006. [\[CrossRef\]](#)
12. Girard, S.; Ouerdane, Y.; Tortech, B.; Marcandella, C.; Robin, T.; Cadier, B.; Baggio, J.; Paillet, P.; Ferlet-Cavrois, V.; Boukenter, A.; et al. Radiation Effects on Ytterbium- and Ytterbium/Erbium-Doped Double-Clad Optical Fibers. *IEEE Trans. Nucl. Sci.* **2009**, *56*, 3293–3299. [\[CrossRef\]](#)
13. Girard, S.; Marcandella, C.; Morana, A.; Perisse, J.; Di Francesca, D.; Paillet, P.; Mace, J.-R.; Boukenter, A.; Leon, M.; Gaillardin, M.; et al. Combined High Dose and Temperature Radiation Effects on Multimode Silica-Based Optical Fibers. *IEEE Trans. Nucl. Sci.* **2013**, *60*, 4305–4313. [\[CrossRef\]](#)
14. Tajitsu, Y.; Ogura, H.; Chiba, A.; Furukawa, T. Investigation of Switching Characteristics of Vinylidene Fluoride/Trifluoroethylene Copolymers in Relation to Their Structures. *Jpn. J. Appl. Phys.* **1987**, *26*, 554. [\[CrossRef\]](#)
15. Imai, H.; Arai, K.; Imagawa, H.; Hosono, H.; Abe, Y. Two types of oxygen-deficient centers in synthetic silica glass. *Phys. Rev. B* **1988**, *38*, 12772–12775. [\[CrossRef\]](#) [\[PubMed\]](#)

16. Galeener, F.L.; Kerwin, D.B.; Miller, A.J.; Mikkelsen, J.J.C. X-ray creation and activation of electron spin resonance in vitreous silica. *Phys. Rev. B* **1993**, *47*, 7760–7779. [[CrossRef](#)] [[PubMed](#)]
17. Griscom, D.L. Radiation hardening of pure-silica-core optical fibers by ultra-high-dose γ -ray pre-irradiation. *J. Appl. Phys.* **1995**, *77*, 5008–5013. [[CrossRef](#)]
18. Wang, T.; Xiao, Z.; Luo, W. Influences of Thermal Annealing Temperatures on Irradiation Induced E' Centers in Silica Glass. *IEEE Trans. Nucl. Sci.* **2008**, *55*, 2685–2688. [[CrossRef](#)]
19. Yeniay, A.; Gao, R. Radiation induced loss properties and hardness enhancement technique for ErYb doped fibers for avionic applications. *Opt. Fiber Technol.* **2013**, *19*, 88–92. [[CrossRef](#)]
20. Hosono, H.; Ikuta, Y.; Kinoshita, T.; Kajihara, K.; Hirano, M. Physical Disorder and Optical Properties in the Vacuum Ultraviolet Region of Amorphous SiO₂. *Phys. Rev. Lett.* **2001**, *87*, 175501. [[CrossRef](#)] [[PubMed](#)]
21. Yin, J.; Wen, J.; Luo, W.; Xiao, Z.; Chen, Z.; Wang, T. Influence of photo- and thermal bleaching on pre-irradiation low water peak single mode fibers. In *SPIE Proceedings, Passive Components and Fiber-Based Devices VIII*; SPIE: Bellingham, WA, USA, 2011; pp. 1–6. [[CrossRef](#)]
22. Mihailov, S.J. Ultrafast laser inscribed fiber Bragg gratings for sensing applications. In *SPIE Proceedings, Fiber Optic Sensors and Applications XIII*; SPIE: Bellingham, WA, USA, 2016; Volume 9852, pp. 173–192. [[CrossRef](#)]
23. Sun, H.-B.; Juodkazis, S.; Watanabe, M.; Matsuo, S.; Misawa, H.; Nishii, J. Generation and Recombination of Defects in Vitreous Silica Induced by Irradiation with a Near-Infrared Femtosecond Laser. *J. Phys. Chem. B* **2000**, *104*, 3450–3455. [[CrossRef](#)]
24. Sudrie, L.; Franco, M.; Prade, B.; Mysyrowicz, A. Study of damage in fused silica induced by ultra-short IR laser pulses. *Opt. Commun.* **2001**, *191*, 333–339. [[CrossRef](#)]
25. Teng, Y.; Zhou, J.; Sharafudeen, K.; Zhou, S.; Miura, K.; Qiu, J. Space-selective crystallization of glass induced by femtosecond laser irradiation. *J. Non Cryst. Solids* **2014**, *383*, 91–96. [[CrossRef](#)]

Disclaimer/Publisher’s Note: The statements, opinions and data contained in all publications are solely those of the individual author(s) and contributor(s) and not of MDPI and/or the editor(s). MDPI and/or the editor(s) disclaim responsibility for any injury to people or property resulting from any ideas, methods, instructions or products referred to in the content.